Received: 7 June 2021 | Revised: 2 December 2021 | Accepted: 8 December 2021 | Published on: 17 January 2022

DOI: 10.1002/qj.4232

Quarterly Journal of the Royal Meteorological Society RMetS

RESEARCH ARTICLE

# Baroclinic instability and large-scale wave propagation in a planetary-scale atmosphere

**Woosok Moon**[1] | **Georgy E. Manucharyan**[2] | **Henk A. Dijkstra**[3]

[1]Nordita, Stockholm University, Stockholm, Sweden

[2]School of Oceanography, University of Washington, Seattle, Washington, USA

[3]Institute for Marine and Atmospheric Research Utrecht, Utrecht University, Utrecht, the Netherlands

**Correspondence**
W. Moon, Nordita, Stockholm University, Roslagstullsbacken 23, 10691 Stockholm, Sweden.
Email: woosok.moon@gmail.com

**Funding information**
Office of Naval Research Global, Grant/Award Number: N00014-19-1-2421; the Ministry of Education, Culture and Science, the Netherlands, Grant/Award Number: 024.002.001; Vetenskapsrådet, Grant/Award Number: 638-2013-9243

**Abstract**

Midlatitude atmospheric variability is dominated by the dynamics of the baroclinically unstable jet stream, which meanders and sheds eddies at the scale of the Rossby deformation radius. The eddies interact with each other and with the jet, affecting the variability on a wide range of scales, but the mechanisms of planetary-scale fluctuations of the jet are not well understood. Here, we develop a theoretical framework to explore the stability of planetary-scale motions in an idealized two-layer model of the atmosphere. The model is based on a combination of vertical shear and the Sverdrup relation, providing the dynamic link between the two layers, with meridional eddy heat fluxes parameterized as a diffusive process with the memory of past baroclinicity of the jet. We find that a planetary-scale instability exists if the vertical shear of the jet does not exceed a particular threshold. The inclusion of the eddy-memory effect enables westward or eastward propagation of planetary waves relative to the barotropic mean flow. Importantly, we find growing planetary waves that propagate slowly westward or are stationary, which could have important implications for the formation of atmospheric blocking events. Our theoretical results suggest that, with ongoing polar amplification due to global warming and the corresponding reduction of the vertical shear of the mean wind, the background conditions for the growth of planetary-scale waves via planetary-scale baroclinic instability are becoming more favorable.

**KEYWORDS**

eddy heat fluxes, eddy memory, low-frequency variability, quasiperiodic oscillation, Southern Hemisphere baroclinic annular mode (BAM), zonal index

## 1 | INTRODUCTION

Planetary-scale waves, the time-scales of which are larger than those of typical weather and smaller than a season (Ghil and Mo, 1991a; 1991b; Screen and Simmonds, 2014), are crucial to shape low-frequency variability in the large-scale atmosphere. Recently, unusual planetary-scale atmospheric motions in the Northern Hemisphere have caused extreme weather events in the midlatitudes, which is considered to be a consequence of ongoing global warming (Petoukhov *et al.*, 2013). The impact of global warming is not equally distributed in the world, but varies region by

region (Cohen, 1990). In particular, the temperature has risen twice as much in high latitudes as in other areas, a phenomenon called Arctic Amplification (AA: Serreze *et al.*, 2009; Pithan and Mauritsen, 2014). AA induces a decrease of baroclinicity in lower levels at midlatitudes in the Northern Hemisphere. It has been suggested that the decrease of baroclinicity is related to the amplified meanders of midlatitude jets leading to extreme weather (Francis and Vavrus, 2012; 2015). However, fluid-dynamical links between the warming of the Arctic region and the weather in the midlatitudes are not revealed clearly, thus one should be cautious to conclude that AA leads to extreme weather in the midlatitudes (Wallace *et al.*, 2014).

Large-scale atmospheric motion in the midlatitudes is governed mainly by the dynamics of jets (Woollings *et al.*, 2010). On weather time-scales, the shear-induced baroclinic instability generates large-scale eddies, growing by taking energy from the mean flow (Pierrehumbert and Swanson, 1995). The growth rate of these synoptic eddies is proportional to the baroclinicity determined by the meridional temperature gradient (Charney, 1947). Traditional baroclinic instability theory, however, is unlikely to explain the current extreme weather events associated with the growth of planetary-scale disturbances. As a matter of fact, AA is lowering the baroclinicity in lower levels in the midlatitudes, which should decrease the activity of synoptic eddies. A new dynamical feature in the planetary-scale atmosphere should be presented to rationalize the contrast between current observations of planetary waves causing extreme weather and the traditional baroclinic instability. It is plausible to guess that the planetary-scale atmosphere, the length-scale of which is larger than synoptic scales, might be governed by different physics, distinct from the major dynamic features of synoptic-scale motions (Phillips, 1963).

Low-frequency variability of the large-scale atmosphere is driven by planetary-scale dynamics, the time-scales of which are larger than those of the weather (Thompson and Wallace, 1998; Hurrell *et al.*, 2003). Planetary-scale motion exists together with synoptic-scale motions in the large-scale atmosphere. It is called "Geostrophic motion type 2" (Phillips, 1963). Several articles introduce derivations of planetary geostrophic motion from the primitive equations by scaling analysis with representative length- and time-scales (Dolaptchiev and Klein, 2009; Pedlosky, 2013; Moon and Cho, 2020). The length-scale for planetary-scale motion is similar to the radius of the Earth, thus various low-frequency phenomena covering the whole hemisphere should be related to planetary geostrophic motion.

An asymptotic approximation for planetary-scale atmospheric motions is the heat equation, with basic dynamical constraints including geostrophic and hydrostatic balances and the Sverdrup relationship derived from the continuity equation (Moon and Cho, 2020). This is quite different on the synoptic scale, where the main evolution equation is derived from a combination of horizontal vorticity dynamics and the heat equation (Pedlosky, 2013). The two scales coexist in the large-scale atmosphere, implying that the governing dynamics in the large-scale atmosphere can be represented by the mutual interaction of the two scales via a multiple-scale analysis. Moon and Cho (2020) emphasize that the contribution of synoptic-scale motions at the planetary scale in the heat equation is represented as the horizontal convergence of the turbulent heat flux of synoptic eddies. According to Phillips (1963), planetary-scale motions should be maintained by external forcing. Therefore, the turbulent heat flux from the synoptic scale acting as one of the external forcings is crucial to shape the overall variability on the planetary scale.

One of the distinct phenomena caused by the interaction of the two scales is a quasi-oscillatory behavior of the meridional heat flux in the Southern Hemisphere (Moon *et al.*, 2021). This variability is called the Baroclinic Annular Mode (BAM), the time period of which is approximately 25 days (Thompson and Barnes, 2014). The planetary-scale dynamics itself cannot explain the oscillatory behavior of the meridional temperature gradient or meridional heat flux, because the mathematical structure of the heat equation is parabolic. Recently, it was suggested that eddy-memory effects in wave–mean interaction in the large-scale ocean could explain the quasi-oscillatory behavior of ocean temperature (Manucharyan *et al.*, 2017). The eddy-memory effect is represented by a kernel integral of the gradient of mean fields with respect to time, which is distinguished from the Fickian approximation parameterizing the turbulent flux of tracers by the instantaneous gradient of the mean field. In particular, if we introduce a finite time integral kernel, the heat equation transforms to a hyperbolic equation, which contains wave propagations and oscillations. Recent work shows that a stochastic oscillator model for the variability of the BAM can be derived by using a finite-time kernel for the parameterization of synoptic-scale turbulent heat flux (Moon *et al.*, 2021).

The transformation of the heat equation into a hyperbolic wave equation by the eddy-memory effect represents, in an approximated way, the generation of planetary-scale waves by nonlinear influences of synoptic eddies on planetary-scale motions. We need to investigate how the planetary-scale waves induced by synoptic eddies are behaving and propagating in the planetary-scale atmosphere. In particular, it is necessary to investigate the existence of a fluid-dynamical instability of planetary-scale waves due to the vertical shear of zonal mean winds. If this instability exists, it might be closely related to

the planetary-scale wiggles generating extreme weather events under ongoing global warming.

In this article, we will adopt the finite-time eddy-memory effect in the planetary heat equation to parameterize the turbulent heat flux of synoptic scales and then study the characteristics of planetary-scale waves induced by the eddy memory. In particular, a vertically sheared flow as a mean flow is considered, to investigate the existence of instability causing the growth of planetary-scale disturbances leading to the increased meandering of the jet stream.

## 2 | LINEAR PLANETARY-SCALE ATMOSPHERIC MOTION WITH EDDY-MEMORY EFFECTS

Large-scale atmospheric motion contains two asymptotic limits: one due to quasigeostrophic motion, the length-scale of which is determined by the internal Rossby deformation radius ($L \sim 1{,}000\,\mathrm{km}$), and a planetary geostrophic one characterized by the external Rossby deformation radius ($L_\mathrm{D} \sim 3{,}000\,\mathrm{km}$) (Moon and Cho, 2020). The external Rossby deformation radius $L_\mathrm{D}$ is defined by $\sqrt{gH}/f$, where $g$ is the acceleration due to gravity, $H$ is a height scale of the atmosphere, and $f$ is the Coriolis parameter.

The planetary geostrophic motion is represented by geostrophic and hydrostatic balances, the Sverdrup relation derived from the continuity equation, and the heat-flux balance:

$$\begin{aligned}
&u_L = -\frac{\partial P_L}{\partial Y},\\
&v_L = \frac{\partial P_L}{\partial X},\\
&\rho_L = -\frac{1}{\rho_\mathrm{s}}\frac{\partial}{\partial z}(\rho_\mathrm{s} P_L),\\
&\frac{1}{\rho_\mathrm{s}}\frac{\partial}{\partial z}(\rho_\mathrm{s} w_L) - \beta_L v_L = 0,\\
&\frac{\partial \Theta_L}{\partial \tau} + u_L\frac{\partial \Theta_L}{\partial X} + v_L\frac{\partial \Theta_L}{\partial Y} + \left(\frac{\partial \Theta_L}{\partial z} + \frac{1}{\epsilon_L \Theta_\mathrm{s}}\frac{d\Theta_\mathrm{s}}{dz}\right) w_L = Q_L,
\end{aligned} \tag{1}$$

where all variables are nondimensionalized using representative scales (Moon and Cho, 2020). Here, $X$ and $Y$ are planetary-scale horizontal coordinates, $z$ is a vertical one, and the time $\tau$ represents planetary-scale time scaled by $U/L_\mathrm{D}$. Here, $U$ is a horizontal velocity scale. The subscript $L$ implies planetary-scale variables. $u_L$, $v_L$, and $w_L$ are $X$, $Y$, and $z$ direction velocities, respectively, and $P_L$ and $\Theta_L$ represent planetary-scale pressure and potential temperature. $\beta_L = (L_\mathrm{D}/a)\cos\theta_0$, where $a$ is the radius of the Earth and $\theta_0$ is a representative midlatitude. $\beta_L \sim \mathcal{O}(1)$ on the planetary scale, while $\beta \sim \mathcal{O}(\epsilon)$ on the synoptic scale, where $\epsilon$ is the Rossby number, defined as $U/fL$, and $\beta$ is defined as $(L/a)\cos\theta_0$. The average vertical profile of the potential temperature is

$$\frac{1}{\Theta_\mathrm{S}}\frac{d\Theta_\mathrm{S}}{dz} \sim \mathcal{O}(\epsilon_L),$$

where $\epsilon_L \equiv U/(fL_\mathrm{D})$ and $\Theta_\mathrm{S}$ is the hemispheric average vertical profile of the potential temperature. $\rho_\mathrm{s}$ is a hemispheric average of air density, thus $\rho_\mathrm{s} = \rho_\mathrm{s}(z)$. $Q_L$ represents the planetary-scale thermal forcing driving the heat-flux balance.

Large-scale atmospheric dynamics can be represented by the mutual interactions of the two scales in a multiscale analysis. Hence, the planetary geostrophic motion is influenced by synoptic-scale eddies and, in particular, the synoptic-scale eddies contribute to horizontal turbulent heat fluxes in the planetary-scale heat equation. On the other hand, the planetary-scale velocities $u_L$, $v_L$, and $w_L$ provide a mean flow for quasigeostrophic vorticity dynamics.

The planetary-scale heat equation with the contribution of synoptic eddies (Moon *et al.*, 2021) is

$$\begin{aligned}
&\frac{\partial \Theta_L}{\partial \tau} + u_L\frac{\partial \Theta_L}{\partial X} + v_L\frac{\partial \Theta_L}{\partial Y} + w_L\left(S + \frac{\partial \Theta_L}{\partial z}\right)\\
&\quad = -\frac{\partial}{\partial x}u_0\theta_0 - \frac{\partial}{\partial y}v_0\theta_0 + Q_L,
\end{aligned} \tag{2}$$

where $x$ and $y$ are synoptic-scale horizontal coordinates and the subscript 0 represents synoptic-scale leading-order variables. $S$ is the static stability, defined by $[1/(\epsilon_L\Theta_\mathrm{S})]d\Theta_\mathrm{S}/dz$. Here, we assume that $S$ is a constant for simplicity. The contribution of synoptic eddies to the planetary-scale heat equation is represented by the horizontal heat flux convergence $-(\partial/\partial x)\overline{u_0\theta_0} - (\partial/\partial y)\overline{v_0\theta_0}$ and the planetary-scale external heat flux $Q_L$ is assumed to be zonally symmetric. The governing equation is constructed based on a dry atmosphere, ignoring the effects of moisture.

To represent the heat equation only by planetary-scale variables, it is required to parameterize the synoptic-scale heat flux using planetary-scale potential temperature. First, we have to do fast-time (synoptic-scale) averaging and spatial averaging over the heat equation. In particular, the spatial derivative in the synoptic scale $\partial/\partial y$ is converted to $\epsilon^{1/2}(\partial/\partial Y)$ by the spatial average, where $L/L_\mathrm{D} \simeq \epsilon^{1/2}$ is used. Here, $L$ is the internal Rossby deformation radius, the basic length-scale for the synoptic motions. Equation 2 becomes

$$\begin{aligned}
&\frac{\partial \Theta_L}{\partial \tau} + u_L\frac{\partial \Theta_L}{\partial X} + v_L\frac{\partial \Theta_L}{\partial Y} + w_L\left(S + \frac{\partial \Theta_L}{\partial z}\right)\\
&\quad = -\epsilon^{1/2}\frac{\partial}{\partial X}\overline{u_0\theta_0} - \epsilon^{1/2}\frac{\partial}{\partial Y}\overline{v_0\theta_0} + Q_L,
\end{aligned} \tag{3}$$

where $\partial/\partial x$ and $\partial/\partial y$ are converted to $\epsilon^{1/2}\partial/\partial X$ and $\epsilon^{1/2}\partial/\partial Y$ by the spatial averaging (Moon *et al.*, 2021). The zonally symmetric thermal forcing $Q_L = Q_L(\tau, Y)$ provides a zonally symmetric mean flow that does not depend upon $X$. Hence, $v_L = w_L = 0$ and there is no advection of potential temperature in the heat equation. The planetary geostrophic motion defined by the zonal wind $u_L^{\mathrm{S}}$, the pressure field $P_L^{\mathrm{S}}$, and the potential temperature $\Theta_L^{\mathrm{S}}$ induced by the zonally symmetric forcing $Q_L$ satisfies

$$\begin{aligned} u_L^{\mathrm{S}} &= -\frac{\partial P_L^{\mathrm{S}}}{\partial Y}, \\ \Theta_L^{\mathrm{S}} &= \frac{\partial P_L^{\mathrm{S}}}{\partial z}, \\ \frac{\partial \Theta_L^{\mathrm{S}}}{\partial \tau} &= Q_L. \end{aligned} \tag{4}$$

A steady-state solution can be obtained from $Q_L(\Theta_L^{\mathrm{S}}) = 0$. $Q_L$ represents thermal forcing, consisting mainly of shortwave and longwave radiative fluxes. When we include local convective processes, $Q_L = 0$ implies a convective radiative equilibrium leading to $\Theta_L^{\mathrm{S}} = \Theta_{\mathrm{E}}$, where $\Theta_{\mathrm{E}}$ is the radiative convective equilibrium temperature (Manabe and Strickler, 1964). The basic balances, $u_L^{\mathrm{S}} = -\partial P_L^{\mathrm{S}}/\partial Y$ and $\Theta_{\mathrm{E}} = \partial P_L^{\mathrm{S}}/\partial z$, can be used to construct a balanced zonal symmetric zonal wind $u_L^{\mathrm{S}}$, which can be the initial velocity field for an idealized global climate model (GCM) dynamic core simulation (Held and Suarez, 1994).

We consider a perturbative potential temperature field $\eta_L$ around the mean potential temperature $\Theta_L^{\mathrm{S}}$. Let $\Theta_L \simeq \Theta_L^{\mathrm{S}} + \epsilon^{1/2}\eta_L$, which is put into Equation 3. The leading-order $\mathcal{O}(1)$ equation becomes the same as Equation 4 and the velocities $v_L$ and $w_L$ are $\mathcal{O}(\epsilon^{1/2})$. Hence, the heat equation to $\mathcal{O}(\epsilon^{1/2})$ is

$$\frac{\partial \eta_L}{\partial \tau} + u_L^{\mathrm{S}}\frac{\partial \eta_L}{\partial X} + v_L\frac{\partial \Theta_L^{\mathrm{S}}}{\partial Y} + w_L S = -\frac{\partial}{\partial X}\overline{u_0\theta_0} - \frac{\partial}{\partial Y}\overline{v_0\theta_0}, \tag{5}$$

where we assume that $\Theta_L^{\mathrm{S}}$ is not dependent on the vertical coordinate $z$, for simplicity.

A closure of Equation 5 requires that the synoptic-scale heat-flux convergence should be parameterized by planetary-scale variables. The meridional temperature gradient $\partial\eta_L/\partial Y$ is dynamically linked with the heat-flux convergence, thus the synoptic-scale heat-flux convergence can be parameterized by a functional form of the meridional potential temperature gradient. In other words, the poleward synoptic heat fluxes act as the primary control of the planetary-scale meridional temperature gradient. Previously, it has been suggested that the meridional heat flux is the result of accumulating baroclinicity during a finite time-scale, which is referred to as the eddy-memory effect (Manucharyan *et al.*, 2017). The eddy-memory effect is used as a mechanism to explain quasi-oscillatory behavior of the large-scale atmosphere and ocean, characterizing subseasonal and multidecadal variability in the atmosphere and ocean, respectively (Jüling *et al.*, 2020; Moon *et al.*, 2021). Following this idea, we can parameterize the meridional heat flux due to synoptic scales as

$$\begin{aligned} \overline{u_0\theta_0} &= -K\frac{\partial}{\partial X}\int_{-\infty}^{\tau}\frac{\eta_L}{r}\exp\left(-\frac{\tau-\tau'}{r}\right)d\tau', \\ \overline{v_0\theta_0} &= -K\frac{\partial}{\partial Y}\int_{-\infty}^{\tau}\frac{\eta_L}{r}\exp\left(-\frac{\tau-\tau'}{r}\right)d\tau', \end{aligned} \tag{6}$$

where $K$ is an eddy diffusivity measuring the intensity of synoptic-scale poleward heat fluxes and $r$ is the time-scale of the eddy memory during which the baroclinicity $\nabla\eta_L$ accumulates to determine the present heat flux by synoptic eddies (Moon *et al.*, 2021).

The equation then becomes

$$\frac{\partial \eta_L}{\partial \tau} + u_L^{\mathrm{S}}\frac{\partial \eta_L}{\partial X} + v_L\frac{\partial \Theta_L^{\mathrm{S}}}{\partial Y} + Sw_L = K\nabla_H^2\eta_L^*, \tag{7}$$

where $\eta_L^*$ satisfies

$$\frac{d\eta_L^*}{d\tau} = -\frac{\eta_L^*}{r} + \frac{\eta_L}{r}. \tag{8}$$

Instead of the original integral kernel (Equation 6), we use the differential Equation 8 in further stability analysis (Manucharyan *et al.*, 2017). Here, the time derivative $d/d\tau$ should be interpreted as the material derivative including the horizontal advection $\overline{u}_L^{\mathrm{S}}$, thus

$$\frac{d}{d\tau} \equiv \frac{\partial}{\partial \tau} + \overline{u}_L^{\mathrm{S}}\frac{\partial}{\partial X}, \tag{9}$$

where $\overline{u}_L^{\mathrm{S}}$ represents the barotropic zonal mean wind, defined as the vertical average of the zonal mean zonal wind, $\overline{u}_L^{\mathrm{S}} \equiv \int_0^1 u_L^{\mathrm{S}} dz$. The last equation needed is the Sverdrup relation connecting the vertical velocity $w_L$ to the meridional velocity $v_L$ due to the planetary beta effect,

$$\frac{\partial w_L}{\partial z} - \frac{1}{H}w_L = \beta_L v_L, \tag{10}$$

where

$$\frac{1}{H} = -\frac{1}{\rho_{\mathrm{S}}}\frac{d\rho_{\mathrm{S}}}{dz}$$

(Moon and Cho, 2020; Moon *et al.*, 2021). Here $\rho_{\mathrm{S}}$ is the hemispheric mean vertical profile of atmospheric density, which is only dependent upon $z$; we also assume that $H$ is a constant.

Taking the $z$-derivative of Equations 7,8, and 10, we obtain

$$\frac{\partial}{\partial\tau}\frac{\partial\eta_L}{\partial z}+u_L^S\frac{\partial}{\partial X}\frac{\partial\eta_L}{\partial z}+S\frac{\partial w_L}{\partial z}=K\nabla_H^2\frac{\partial\eta_L^*}{\partial z}, \tag{11}$$

$$\frac{\partial^2 w_L}{\partial z^2}-\frac{1}{H}\frac{\partial w_L}{\partial z}=\beta_L\frac{\partial\eta_L}{\partial X}, \tag{12}$$

$$\frac{d}{d\tau}\frac{\partial\eta_L^*}{\partial z}+\frac{1}{r}\frac{\partial\eta_L^*}{\partial z}=\frac{1}{r}\frac{\partial\eta_L}{\partial z}, \tag{13}$$

where Equation 11 is obtained using the thermal wind balance,

$$\begin{aligned}\frac{\partial u_L^S}{\partial z}&=-\frac{\partial\Theta_L^S}{\partial y},\\ \frac{\partial v_L}{\partial z}&=\frac{\partial\eta_L}{\partial X},\end{aligned} \tag{14}$$

leading to

$$\frac{\partial u_L^S}{\partial z}\frac{\partial\eta_L}{\partial X}+\frac{\partial v_L}{\partial z}\frac{\partial\Theta_L^S}{\partial Y}=0. \tag{15}$$

Next, we will convert the above equations (Equations 11–13) to a two-layer model with the boundary conditions $w_L=0$ at $z=0$ and $z=1$, where $z=1$ implies the top layer, where synoptic baroclinic waves break and momentum flux is dominant. It is a hypothetical situation, assuming that the tropopause is a fixed surface. The baroclinic instability problem on the $f$-plane in quasigeostrophic motion also used this boundary condition (Eady, 1949; Dolaptchiev and Klein, 2009). Taking the $z$-derivative is critical to construct a two-layer model. Without the $z$-derivative, the main variable is the anomalous pressure $\psi_L$ satisfying $\partial\psi_L/\partial z=\eta_L$, in which case we need at least three layers. For simplicity in the further analytical approach, it is desirable to rely on the two-layer model. However, if we want to include nonlinear terms, taking the $z$-derivative does not lead to more simplicity.

## 3 | TWO-LAYER LINEAR PLANETARY-SCALE ATMOSPHERIC MODEL

Layer models have been widely used in large-scale atmospheric and oceanic dynamics (Pedlosky, 2013). Layer models in the vertical coordinate have major dynamic features in sheared flows in the large-scale atmosphere and ocean (Figure 1). This means one can avoid dealing with complicated special functions in eigenvalue problems in the vertical coordinate, such as the confluent hypergeometric function used in the original baroclinic instability theory(Charney, 1947). In particular, two-layer models have been applied in many directions for quasigeostrophic motions in the atmosphere including baroclinic instability (Phillips, 1951).

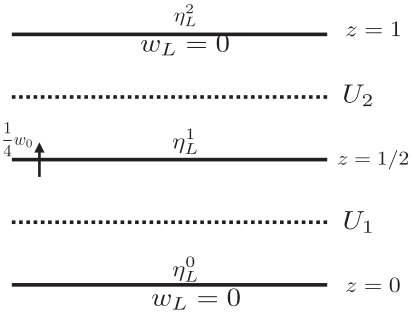


**FIGURE 1** The schematic of the two-layer model. The surface and top of the atmosphere are represented as $z=0$ and $z=1$, respectively. The two layers are applied at $z=1/4$ and $z=3/4$, where the zonal mean winds are specified as $U_1$ and $U_2$. Potential temperature anomalies at $z=0, z=1/2$, and $z=1$ are $\eta_L^0$, $\eta_L^1$, and $\eta_L^2$, respectively. Boundary conditions are imposed on the vertical velocity $w_L$, hence $w_L=0$ at $z=0$ and $z=1$. The vertical velocity at the middle level $z=1/2$ is $\frac{1}{4}w_0$

Here we introduce a two-layer model for the linear planetary geostrophic motion represented by Equation 7. The vertical coordinate $z$ goes from $z=0$ to $z=1$, representing the surface and top of the atmosphere, respectively. The main equations in Equation 7 are approximated at two levels $z=1/4$ and $z=3/4$. Imposed boundary conditions are $w_L=0$ at $z=0,1$. The potential temperature anomaly $\eta_L$ is represented by $\eta_L^0$ at $z=0$, $\eta_L^1$ at $z=1/2$, and $\eta_L^2$ at $z=1$. The zonal mean wind $U$ is $U_1$ at $z=1/4$ and $U_2$ at $z=3/4$. The existence of vertical shear means $U_2-U_1=\Delta U$ is positive, in agreement with observations at midlatitudes.

### 3.1 | Sverdrup relationship

The Sverdrup relationship (Equation 8) connects the vertical velocity $w_L$ to the potential temperature anomaly $\eta_L$. First of all, for a simple expression of the vertical velocity $w_L$, let us assume that $w_L=w_0(X,Y)z(1-z)$, which satisfies the boundary conditions at $z=0$ and $z=1$. This could be understood as a minimal expression of the vertical structure of $w_L$. Hence, $\partial w_L/\partial z=w_0-2w_0z$ and $\partial^2 w_L/\partial z^2=-2w_0$. Now, Equation 12 at $z=1/4$ is approximated by

$$-2w_0-\frac{1}{2H}w_0=\frac{1}{2}\beta_L\frac{\partial}{\partial X}\left(\eta_L^1+\eta_L^0\right). \tag{16}$$

In the same way, at $z = 3/4$, we have

$$-2w_0 + \frac{1}{2H}w_0 = \frac{1}{2}\beta_L \frac{\partial}{\partial X}\left(\eta_L^2 + \eta_L^1\right). \tag{17}$$

Here, we approximate $\eta_L$ at $z = 1/4$ ($z = 3/4$) as an average of $\eta_L^0$ and $\eta_L^1$ ($\eta_L^1$ and $\eta_L^2$). Subtracting Equation 16 from Equation 17 gives

$$w_0 = \frac{1}{4}\beta_L H \frac{\partial}{\partial X}(q_1 + q_2), \tag{18}$$

where

$$\begin{aligned} q_1 &= \frac{\partial \eta_L}{\partial z}|_{z=1/4} \simeq 2\left(\eta_L^1 - \eta_L^0\right), \\ q_2 &= \frac{\partial \eta_L}{\partial z}|_{z=3/4} \simeq 2\left(\eta_L^2 - \eta_L^1\right). \end{aligned} \tag{19}$$

### 3.2 | Linear heat equation

The Sverdrup relationship tells us that $\partial w_L/\partial z = \frac{1}{2}w_0$ at $z = 1/4$ and $\partial w_L/\partial z = -\frac{1}{2}w_0$ at $z = 3/4$. Equation 11 is approximated at both $z = 1/4$ and $z = 3/4$, yielding

$$\frac{\partial}{\partial \tau}q_1 + U_1\frac{\partial}{\partial X}q_1 + p\frac{\partial}{\partial X}(q_1 + q_2) = K\nabla_H^2 q_1^*, \tag{20}$$

$$\frac{\partial}{\partial \tau}q_2 + U_2\frac{\partial}{\partial X}q_2 - p\frac{\partial}{\partial X}(q_1 + q_2) = K\nabla_H^2 q_2^*, \tag{21}$$

where $p = \frac{1}{8}\beta_L SH$ is a measure of static stability and $q_1^*$ and $q_2^*$ satisfy

$$\left(\frac{\partial}{\partial \tau} + \overline{U}\frac{\partial}{\partial X} + \frac{1}{r}\right)q_{1,2}^* = \frac{q_{1,2}}{r}, \tag{22}$$

where $\overline{U} \equiv \frac{1}{2}(U_1 + U_2)$ represents the mean barotropic zonal wind velocity. Equation 22 is inserted into Equations 20 and 21. Finally, we have

$$\begin{aligned} &\left(\frac{\partial}{\partial \tau} + \overline{U}\frac{\partial}{\partial X} + \frac{1}{r}\right)\left(\frac{\partial}{\partial \tau} + U_1\frac{\partial}{\partial X}\right)q_1 \\ &\quad + p\frac{\partial}{\partial X}\left(\frac{\partial}{\partial \tau} + \overline{U}\frac{\partial}{\partial X} + \frac{1}{r}\right)(q_1 + q_2) = \frac{K}{r}\nabla_H^2 q_1, \end{aligned} \tag{23}$$

$$\begin{aligned} &\left(\frac{\partial}{\partial \tau} + \overline{U}\frac{\partial}{\partial X} + \frac{1}{r}\right)\left(\frac{\partial}{\partial \tau} + U_2\frac{\partial}{\partial X}\right)q_2 \\ &\quad - p\frac{\partial}{\partial X}\left(\frac{\partial}{\partial \tau} + \overline{U}\frac{\partial}{\partial X} + \frac{1}{r}\right)(q_1 + q_2) = \frac{K}{r}\nabla_H^2 q_2. \end{aligned} \tag{24}$$

It should be emphasized that the eddy-memory effect represented in Equation 22 changes the mathematical structure of the main Equations 20 and 21. Without the eddy-memory effect, Equations 20 and 21 are parabolic partial differential equations, the solutions of which show diffusion from an initial source with advection. The inclusion of a finite-size eddy memory transforms the main equations from parabolic to hyperbolic ones. This is critical to generate planetary-size eddies propagating against the mean westerlies. Now, we can introduce the barotropic mode $\overline{q} = \frac{1}{2}(q_1 + q_2)$ and the baroclinic mode $\Delta q = \frac{1}{2}(q_2 - q_1)$ and obtain

$$\begin{aligned} &\left(\frac{\partial}{\partial \tau} + \overline{U}\frac{\partial}{\partial X} + \frac{1}{r}\right)\left(\frac{\partial}{\partial \tau} + \overline{U}\frac{\partial}{\partial X}\right)\overline{q} \\ &\quad + \frac{1}{2}\Delta U\frac{\partial}{\partial X}\left(\frac{\partial}{\partial \tau} + \overline{U}\frac{\partial}{\partial X} + \frac{1}{r}\right)\Delta q = \frac{K}{r}\nabla_H^2 \overline{q}, \end{aligned} \tag{25}$$

$$\begin{aligned} &\frac{1}{2}(\Delta U - 4p)\frac{\partial}{\partial X}\left(\frac{\partial}{\partial \tau} + \overline{U}\frac{\partial}{\partial X} + \frac{1}{r}\right)\overline{q} \\ &\quad \left(\frac{\partial}{\partial \tau} + \overline{U}\frac{\partial}{\partial X} + \frac{1}{r}\right)\left(\frac{\partial}{\partial \tau} + \overline{U}\frac{\partial}{\partial X}\right)\Delta q = \frac{K}{r}\nabla_H^2 \Delta q, \end{aligned} \tag{26}$$

where $\Delta U = U_2 - U_1$.

## 4 | NORMAL MODE ANALYSIS

Assume that the horizontal domain is a channel bounded in the $Y$-direction with the boundary condition $q_{1,2} = 0$ at $Y = 0$ and $Y = 1$. Let $\{\overline{q}, \Delta q\} = \{\overline{Q}, \Delta Q\}e^{\sigma\tau}e^{ikX}\sin(lY)$, where $\overline{Q}$ and $\Delta Q$ are the amplitudes of the barotropic and baroclinic modes, respectively, $k$ and $l$ are $X$ and $Y$ direction wave numbers, and $\sigma$ is a growth rate of barotropic/baroclinic modes. This leads to

$$\left(x^2 - \frac{1}{4r^2} + \frac{K}{r}(k^2 + l^2)\right)\overline{Q} + \frac{1}{2}ikx\Delta U\Delta Q = 0, \tag{27}$$

$$\frac{1}{2}ikx(\Delta U - 4p)\overline{Q} + \left(x^2 - \frac{1}{4r^2} + \frac{K}{r}(k^2 + l^2)\right)\Delta Q = 0, \tag{28}$$

where $x = \sigma + ik\overline{U} + 1/2r$. For nontrivial solutions,

$$\left(x^2 - \frac{1}{4r^2} + \frac{K}{r}(k^2 + l^2)\right)^2 = k^2\left(p\Delta U - \frac{1}{4}\Delta U^2\right)x^2. \tag{29}$$

Here the sign of the term $p\Delta U - \frac{1}{4}\Delta U^2$ is quite important to characterize the solutions. We have to consider two cases, depending on the sign of this term.

### 4.1 | Low wind shear case ($0 \le \Delta U \le 4p$)

This range of the $\Delta U$ implies that $p\Delta U - \frac{1}{4}\Delta U^2 > 0$. Let $b^2 \equiv p\Delta U - \frac{1}{4}\Delta U^2$, which leads to

$$x^2 - \frac{1}{4r^2} + \frac{K}{r}(k^2 + l^2) = \pm\frac{1}{2}bkx, \tag{30}$$

where $x = \sigma + ik\overline{U} + 1/2r$. There are four solutions representing dispersion relationships containing the growth and phase of planetary waves:

$$\sigma_{1,2} = \frac{1}{4}bk - \frac{1}{2r} - ik\overline{U} \pm \sqrt{\frac{1}{4r^2} + \frac{1}{16}b^2k^2 - \frac{K}{r}(k^2+l^2)}, \tag{31}$$

$$\sigma_{3,4} = -\frac{1}{4}bk - \frac{1}{2r} - ik\overline{U} \pm \sqrt{\frac{1}{4r^2} + \frac{1}{16}b^2k^2 - \frac{K}{r}(k^2+l^2)}, \tag{32}$$

where $\mathrm{Re}(\sigma)$ is the growth rate of waves and $-\mathrm{Im}(\sigma)/k$ is the $x$-direction phase speed $C_x$.

Furthermore, the sign of the term inside the square root is important to determine the characteristics of waves. When the sign is positive, the waves have a phase velocity the same as the mean wind $\overline{U}$ and the square-root term contributes to the growth rate. On the other hand, when the sign is negative, the square-root term contributes to the phase velocity, thus the waves propagate westward or eastward with respect to the mean wind.

When

$$\frac{K}{r}(k^2+l^2) < \frac{1}{4r^2} + \frac{1}{16}b^2k^2,$$

the growth rates of the waves are

$$\mathrm{Re}(\sigma_{1,2}) = \frac{1}{4}bk - \frac{1}{2r} \pm \sqrt{\frac{1}{4r^2} + \frac{1}{16}b^2k^2 - \frac{K}{r}(k^2+l^2)}, \tag{33}$$

$$\mathrm{Re}(\sigma_{3,4}) = -\frac{1}{4}bk - \frac{1}{2r} \pm \sqrt{\frac{1}{4r^2} + \frac{1}{16}b^2k^2 - \frac{K}{r}(k^2+l^2)}, \tag{34}$$

and the $x$-direction phase velocities are

$$C_x^{1,2,3,4} = \overline{U}. \tag{35}$$

The waves represented by $\sigma_{1,2}$ grow in time due to the contribution of $\frac{1}{4}bk$ overcoming the decay controlled by the eddy memory $-1/(2r)$. The square-root term contributes to the growth rate positively ($\sigma_1$) or negatively ($\sigma_2$). The waves described by $\sigma_{3,4}$ have a dominant negative contribution from $-\frac{1}{4}bk$, implying that these waves decay quickly.

However, when

$$\frac{K}{r}(k^2+l^2) > \frac{1}{4r^2} + \frac{1}{16}b^2k^2,$$

the growth rates are

$$\mathrm{Re}(\sigma_{1,2}) = \frac{1}{4}bk - \frac{1}{2r}, \tag{36}$$

$$\mathrm{Re}(\sigma_{3,4}) = -\frac{1}{4}bk - \frac{1}{2r}. \tag{37}$$

The magnitude of the waves $\sigma_{1,2}$ increases when $k$ is larger than $2/(br)$, but the waves $\sigma_{3,4}$ decay in time for all $k$. The phase velocities are

$$C_x^{1,3} = \overline{U} - \frac{1}{k}\sqrt{\frac{K}{r}(k^2+l^2) - \frac{1}{4r^2} - \frac{1}{16}b^2k^2}, \tag{38}$$

$$C_x^{2,4} = \overline{U} + \frac{1}{k}\sqrt{\frac{K}{r}(k^2+l^2) - \frac{1}{4r^2} - \frac{1}{16}b^2k^2}. \tag{39}$$

Here, $C_x^{1,3}$ ($C_x^{2,4}$) represent waves propagating westward (eastward) with respect to the mean wind. In particular, with a proper choice of $r$ and $K$, $C_x^{1,3}$ can represent stationary waves with certain $k$ values, in which case $\sigma_1$ implies a perturbation growing in time while being almost stationary.

Figure 2 shows the growth rates (top panel) and the phase speeds (bottom panel) dependent on the wavenumber $k$ when the memory $r$ is equal to (a) 0.25 and (b) 2. Except for the memory $r$, other parameters are the same for the two cases. First of all, when the memory is short ($r = 0.25$), waves with lower $k$ propagate with the mean wind ($\overline{U} = 1.0$), but no waves grow in time. As $k$ increases and becomes larger than $\sim 3$, the waves $\sigma_{1,2}$ become unstable and grow in time. While the wave $\sigma_2$ moves eastward faster than the mean wind, the wave $\sigma_1$ is almost stationary or moving westward very slowly. The other waves $\sigma_{3,4}$ decay more quickly with higher wavenumbers. On the other hand, when the memory is long ($r = 2.0$) (Figure 2b), even for long waves (small wavenumber) there are waves growing in time ($\sigma_{1,2}$). One of them, $\sigma_1$, moves eastward but more slowly than the mean wind, and the other, $\sigma_2$, moves faster than the mean wind. As the wavenumber increases, the waves $\sigma_{1,2}$ grow even faster, but the phase speed becomes equal to the mean wind.

All variables are nondimensionalized. The length-scale is the external Rossby deformation radius $L_\mathrm{D}$, which is around 3,000 km in the midlatitudes, and the horizontal velocity scale $U$ is around 10 m·s$^{-1}$. Thus, the unit time is set up as the advective time-scale $L_\mathrm{D}/U$, which is around 3 days. Hence, the short memory $r = 0.25$ implies around 0.75 days and the long memory $r = 2$ around 6 days. The eddy memory $r$ may vary case by case, even though the average value is close to 4 days in the Southern Hemisphere

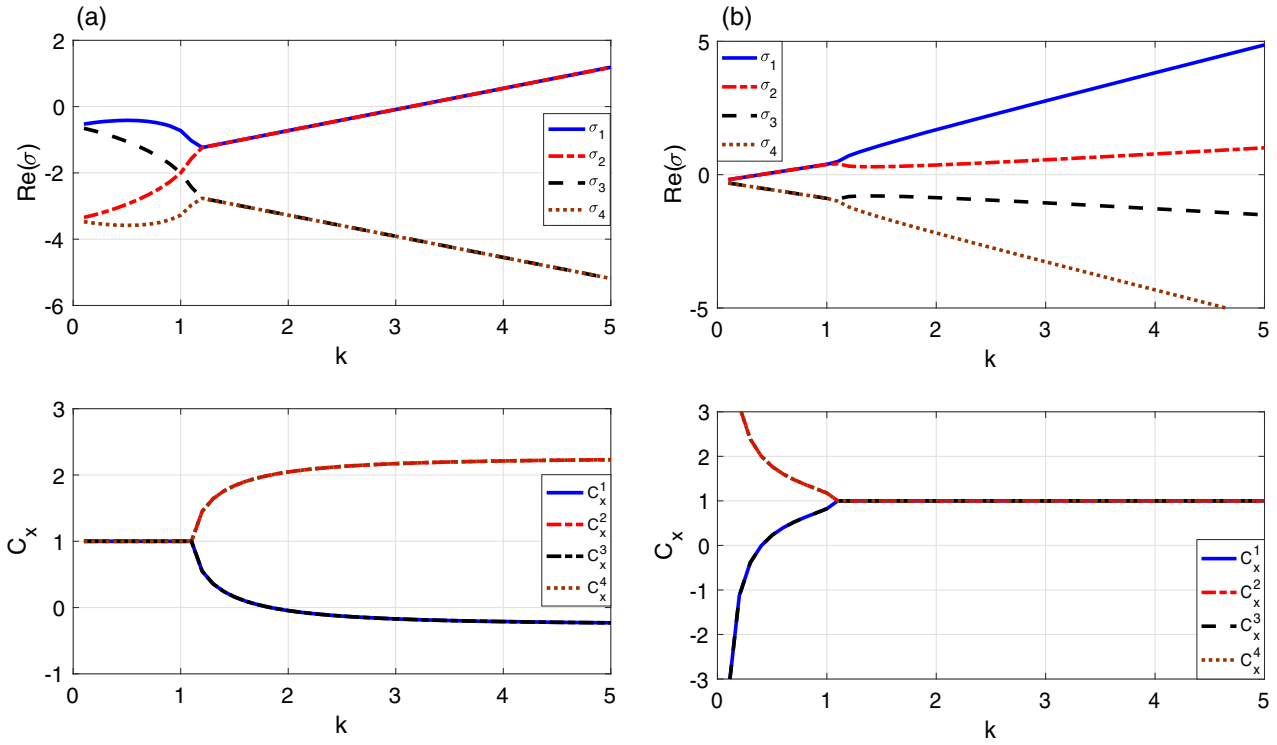


**FIGURE 2** The growth rate of four waves $\sigma_{1,2,3,4}$ (top panel) and the $x$-direction phase velocities $C_x^{1,2,3,4}$ (bottom panel) when (a) $r = 0.25$ and (b) $r = 2$. $p = 0.8$, $\Delta U = 1.5$, $\overline{U} = 1.0$, $l = 1$, and $K = 0.5$ are commonly applied to both cases [Colour figure can be viewed at wileyonlinelibrary.com]

(Moon *et al.*, 2021). Here, we investigate the behavior of normal modes with various values of $r$ around the average value in the Southern Hemisphere, where $\Delta U = 1.5$ implies $dU/dz = 3\ \mathrm{m{\cdot}s^{-1}}\ \cdot\mathrm{km^{-1}}$ when we use a vertical length-scale $H = 5\,\mathrm{km}$. Phillips (1954) uses the quasi-geostrophic equation in a two-level model to investigate the barolinic instability in the midlatitudes. According to his result, when $dU/dz = 3\ \mathrm{m{\cdot}s^{-1}}\ \cdot\mathrm{km^{-1}}$, the fastest growing wave reaches twice its original magnitude in 1.5 days, which is equivalent to $\mathrm{Re}(\sigma) \simeq 1.4$. The two cases in Figure 2 show similar or smaller growth rate compared with that of synoptic eddies when $k$ is smaller than 4.

## 4.2 | High wind shear case ($\Delta U > 4p$)

If the vertical shear is above the threshold $4p$, the right side of Equation 29 becomes negative. Let $d^2 = -p\Delta U + \frac{1}{4}\Delta U^2$ and then we obtain

$$x^2 - \frac{1}{4r^2} + \frac{K}{r}(k^2 + l^2) = \pm\frac{1}{2}idkx. \tag{40}$$

The following dispersion relations are

$$\sigma_{1,2} = -\frac{1}{2r} - ik\overline{U} + i\frac{1}{4}dk \pm \sqrt{\frac{1}{4r^2} - \frac{1}{16}d^2k^2 - \frac{K}{r}(k^2 + l^2)}, \tag{41}$$

$$\sigma_{3,4} = -\frac{1}{2r} - ik\overline{U} - i\frac{1}{4}dk \pm \sqrt{\frac{1}{4r^2} - \frac{1}{16}d^2k^2 - \frac{K}{r}(k^2 + l^2)}. \tag{42}$$

The determination of growth rate and phase speed is also dependent upon the sign of the term inside the square root. When

$$\frac{K}{r}(k^2 + l^2) < \frac{1}{4r^2} - \frac{1}{16}d^2k^2,$$

the growth rates are

$$\mathrm{Re}\sigma_{1,3} = -\frac{1}{2r} + \sqrt{\frac{1}{4r^2} - \frac{1}{16}d^2k^2 - \frac{K}{r}(k^2 + l^2)}, \tag{43}$$

$$\mathrm{Re}\sigma_{2,4} = -\frac{1}{2r} - \sqrt{\frac{1}{4r^2} - \frac{1}{16}d^2k^2 - \frac{K}{r}(k^2 + l^2)}, \tag{44}$$

and the following phase velocities are

$$C_x^{1,2} = \overline{U} - \frac{1}{4}d, \tag{45}$$

$$C_x^{3,4} = \overline{U} + \frac{1}{4}d. \tag{46}$$

According to the phase velocities, there are waves propagating westward ($C_x^{1,2}$) and eastward ($C_x^{3,4}$) with

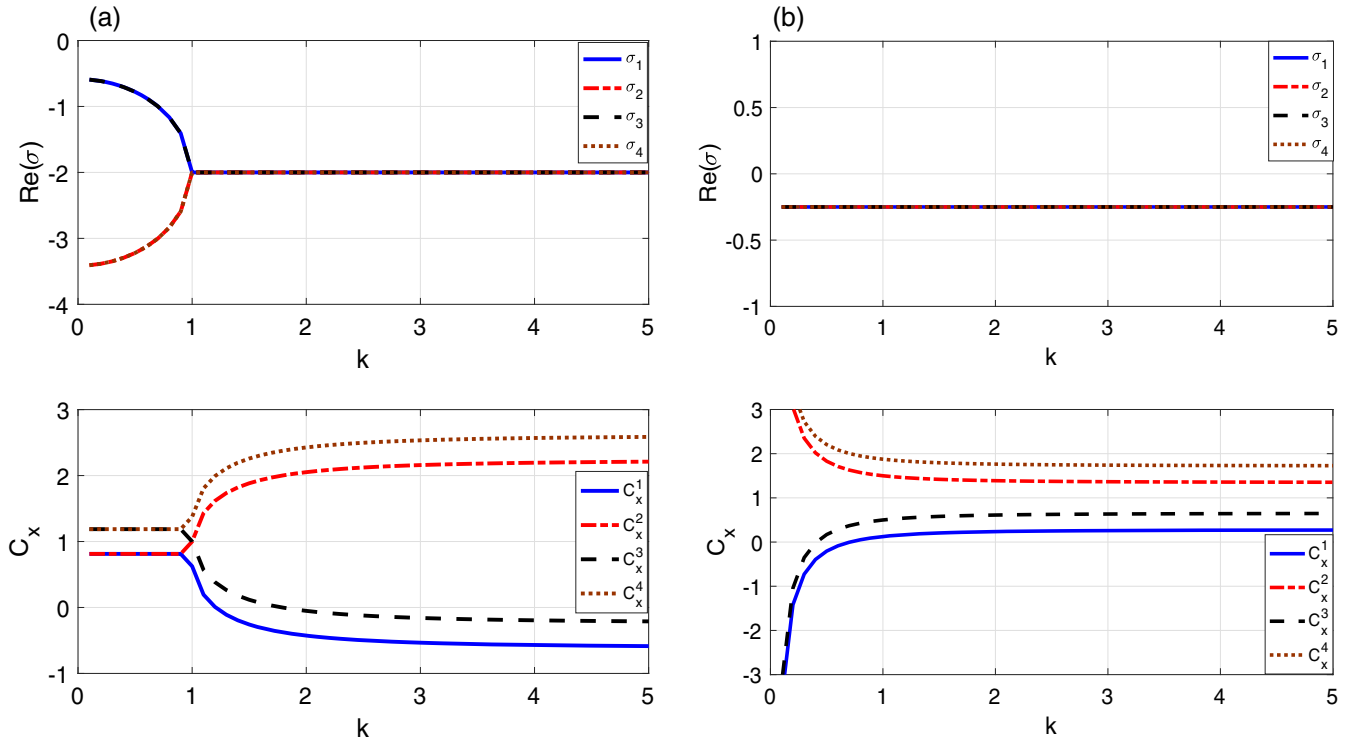


**FIGURE 3** Same as Figure 2, except for $p = 0.25$, thus $4p - \Delta U < 0$. We also consider (a) a short memory case ($r = 0.25$) and (b) a long memory case ($r = 2$) [Colour figure can be viewed at wileyonlinelibrary.com]

respect to the mean wind ($\overline{U}$). The growth rates show that the four waves decay in time, mainly due to the eddy-memory effect represented by $-1/(2r)$.

Similarly, when

$$\frac{K}{r}\left(k^2 + l^2\right) > \frac{1}{4r^2} - \frac{1}{16}d^2k^2,$$

all four waves have the same growth rate $-1/(2r)$, representing the effect of finite eddy memory. The following phase velocities are

$$C_x^{1,2} = \overline{U} - \frac{1}{4}d \pm \frac{1}{k}\sqrt{\frac{K}{r}(k^2 + l^2) + \frac{1}{16}d^2k^2 - \frac{1}{4r^2}}, \quad (47)$$

$$C_x^{3,4} = \overline{U} + \frac{1}{4}d \pm \frac{1}{k}\sqrt{\frac{K}{r}(k^2 + l^2) + \frac{1}{16}d^2k^2 - \frac{1}{4r^2}}, \quad (48)$$

representing various waves propagating westward or eastward with respect to the mean wind.

Figure 3 shows the growth rates and phase velocities of four waves when the memory is (a) short ($r = 0.25$) and (b) long ($r = 2$). Short memory implies faster decay for all waves. In terms of propagation, two kinds of waves exist. One type propagates eastwards faster than the mean wind ($C_x^{2,4}$) and the other is almost stationary or moves westward slowly ($C_x^{1,3}$). Long memory implies slow decay. All waves decay with the same rate controlled by the finite eddy-memory effect. There are also two kinds of waves in terms of propagation, similar to the short memory case. Two waves ($C_x^{2,4}$) propagate eastwards faster than the mean wind and the other two ($C_x^{1,3}$) propagate eastward more slowly than the mean wind.

## 5 | DISCUSSION

### 5.1 | Role of the eddy memory

Above, we considered the case in which the poleward heat flux of synoptic eddies is the result of the finite eddy memory. To investigate the role of the eddy memory for westward-propagating unstable waves, let us consider the case with no eddy memory. No memory follows from the limit $r \to 0$ in Equation 22, which leads to $q_{1,2}^* = q_{1,2}$. This means the recovery of the Fickian approximation. The two-layer equations (Equations 20 and 21) become

$$\frac{\partial}{\partial\tau}q_1 + U_1\frac{\partial}{\partial X}q_1 + p\frac{\partial}{\partial X}(q_1 + q_2) = K\nabla_H^2 q_1, \quad (49)$$

$$\frac{\partial}{\partial\tau}q_2 + U_2\frac{\partial}{\partial X}q_2 - p\frac{\partial}{\partial X}(q_1 + q_2) = K\nabla_H^2 q_2. \quad (50)$$

A normal mode analysis setting $q_{1,2} = \hat{q}_{1,2} e^{\sigma\tau} e^{ikX} \sin(lY)$ leads to

$$(\sigma + ikU_1 + ikp + K(k^2 + l^2))\hat{q}_1 + ikp\hat{q}_2 = 0, \quad (51)$$

$$-ikp\hat{q}_1 + (\sigma + ikU_2 - ikp + K(k^2 + l^2))\hat{q}_2 = 0, \quad (52)$$

where the characteristic equation is

$$(\sigma + ik\overline{U} + K(k^2 + l^2))^2 = k^2\left(-\frac{1}{4}\Delta U^2 + p\Delta U\right). \quad (53)$$

For $0 < \Delta U < 4p$, we find

$$\sigma = -K(k^2 + l^2) \pm bk - ik\overline{U}, \quad (54)$$

where $b^2 = -\frac{1}{4}\Delta U^2 + p\Delta U$. This dispersion relationship represents waves with phase speeds $\overline{U}$ and growth rates $-K(k^2 + l^2) \pm bk$. If $bk > K(k^2 + l^2)$, the waves grow in time, but if the diffusion is larger, the waves decay exponentially in time. The phase speed is the same as the mean wind, which implies that the waves are advected by the mean wind. When $\Delta U > 4p$,

$$\sigma = -K(k^2 + l^2) + ik(\overline{U} \pm d), \quad (55)$$

where $d^2 = -\frac{1}{4}\Delta U^2 + p\Delta U$. Here the two waves decay in time. Without the eddy memory, it is impossible to find unstable or almost neutral waves propagating against the mean wind. The eddy-memory effect is hence crucial to generate planetary-scale unstable waves propagating westwards or eastwards with respect to the zonal mean wind.

This situation can be understood more easily from a simple flux equation:

$$\frac{\partial \overline{C}}{\partial t} = -\nabla \cdot \overline{\mathbf{u}'C'}, \quad (56)$$

where $\overline{C}$ is the mean of a tracer $C$, $C'$ is the deviation from the mean, and $\mathbf{u}$ is the velocity of the flow. The Fickian approximation implies that $\overline{\mathbf{u}'C'} \simeq -K\nabla\overline{C}$ with diffusivity $K$. This leads to a parabolic partial differential equation,

$$\frac{\partial \overline{C}}{\partial t} = K\nabla^2\overline{C}, \quad (57)$$

where the solution $\overline{C}$ diffuses away from an initial source. If a linear advection $U\nabla\overline{C}$ is included in the above parabolic equation, the initial source follows the mean wind $U$ and diffuses away. This represents the case without eddy memory.

The finite memory effect is represented by

$$\frac{\partial}{\partial t}\overline{\mathbf{u}'C'} = -K\nabla\overline{C} - \frac{\overline{\mathbf{u}'C'}}{r}, \quad (58)$$

where $r$ is the eddy-memory strength. Combining it with the main Equation 56, we have

$$\frac{\partial^2 \overline{C}}{\partial t^2} + \frac{1}{r}\frac{\partial \overline{C}}{\partial t} = K\nabla^2\overline{C}. \quad (59)$$

This is a damped wave equation describing the propagation of fluctuations with damping. The inclusion of the memory changes the mathematical structure of the main equation from parabolic to hyperbolic. Propagation against a mean wind is possible, which is essential to observe growing stationary planetary-scale waves overcoming the mean westerlies.

## 5.2 | Growth mechanism

### 5.2.1 | Vertical shear and the Sverdrup relationship

The time growth of a perturbation should be explained by the combination of the baroclinic mean field and the Sverdrup relationship. We can investigate the dynamic role of the two processes systematically in the two-layer model.

Consider a pure shear flow without any other physical process. Here, $U_1 = -\frac{1}{2}\Delta U$ and $U_2 = \frac{1}{2}\Delta U$. The governing equations in the two-layer model are then

$$\begin{aligned} \frac{\partial}{\partial\tau}q_1 - \frac{1}{2}\Delta U\frac{\partial}{\partial X}q_1 = 0, \\ \frac{\partial}{\partial\tau}q_2 + \frac{1}{2}\Delta U\frac{\partial}{\partial X}q_2 = 0, \end{aligned} \quad (60)$$

which is equivalent to

$$\begin{aligned} \frac{\partial}{\partial\tau}\overline{q} - \frac{1}{4}\Delta U\frac{\partial}{\partial X}\Delta q = 0, \\ \frac{\partial}{\partial\tau}\Delta q - \Delta U\frac{\partial}{\partial X}\overline{q} = 0, \end{aligned} \quad (61)$$

where $\overline{q} = \frac{1}{2}(q_1 + q_2)$ and $\Delta q = q_1 - q_2$. This leads to

$$\frac{\partial^2}{\partial\tau^2}\overline{q} - \frac{1}{4}\Delta U^2\frac{\partial^2}{\partial X^2}\overline{q} = 0, \quad (62)$$

The final equation represents a wave equation with wave solutions propagating with the velocity $\pm\frac{1}{2}\Delta U$.

The equations with the contribution of the Sverdrup relationship $p\frac{\partial}{\partial X}(q_1 + q_2)$ are

$$\begin{aligned} \frac{\partial}{\partial\tau}\overline{q} - \frac{1}{4}\Delta U\frac{\partial}{\partial X}\Delta q = 0, \\ \frac{\partial}{\partial\tau}\Delta q - (\Delta U - 4p)\frac{\partial}{\partial X}\overline{q} = 0, \end{aligned} \quad (63)$$

which leads to

$$\frac{\partial^2}{\partial \tau^2}\overline{q} + \left(-\frac{1}{4}\Delta U^2 + p\Delta U\right)\frac{\partial^2}{\partial X^2}\overline{q} = 0. \tag{64}$$

Compared with Equation 62, the term $p\Delta U$ slows down the propagation of planetary waves. The interaction between the two layers hinders the propagation of perturbations forced by the vertical shear. However, only when $-\frac{1}{4}\Delta U^2 + p\Delta U < 0$ do the wave characteristics remain as the main feature; when $-\frac{1}{4}\Delta U^2 + p\Delta U > 0$, that is, $\Delta U < 4p$, Equation 64 changes its dynamic characteristics from the propagation of waves to the growth of perturbations. The Sverdrup relationship, which describes the interactions between the vertical layers, provides a way to use the available potential energy stored in the vertical shear of the mean wind for the growth of a perturbation when the shear is below the threshold.

Figure 4 describes the mechanisms of the behavior of wave perturbations using a schematic. The evolution equation,

$$\frac{\partial q}{\partial \tau} = -U\frac{\partial q}{\partial X} - S\frac{\partial w_L}{\partial z},$$

tells us that $q$ is temporarily updated by the horizontal advection $-U(\partial q/\partial X)$ and the contribution from the Sverdrup relation $-S(\partial w_L/\partial z)$. The horizontal advection has opposite effects on the two levels, due to the vertical shear, and the Sverdrup relation provides a dynamical link between the two levels through the vertical velocity $w_L$. The temporal change of $q$ is determined by the competition between the two contributions. Hence, determining which process is more dominant is crucial to determine the overall growth of a given perturbation. We will describe below how an initial disturbance $q_2$ at the upper level evolves due to the Sverdrup relation and horizontal advection. It starts from an initial disturbance given as $q_2 \neq 0$ and $q_1 = 0$. Hence, the barotropic mode $\overline{q} \equiv \frac{1}{2}(q_1 + q_2)$ is equal to $\frac{1}{2}q_2$. The barotropic mode can be interpreted as the estimation of $q$ at the middle level $z = \frac{1}{2}$. Dynamically, $q$ is understood as part of the planetary potential vorticity, which is $\partial\eta/\partial z - \eta/(SH)$. Thus $q = \partial\eta/\partial z$ contributes to the planetary-scale vorticity at each layer (Figure 4a). Positive (negative) perturbation of $q$ generates cyclonic (anticyclonic) motion in the middle ($z = 1/2$) of the vertical domain, which induces a meridional velocity $v$, which

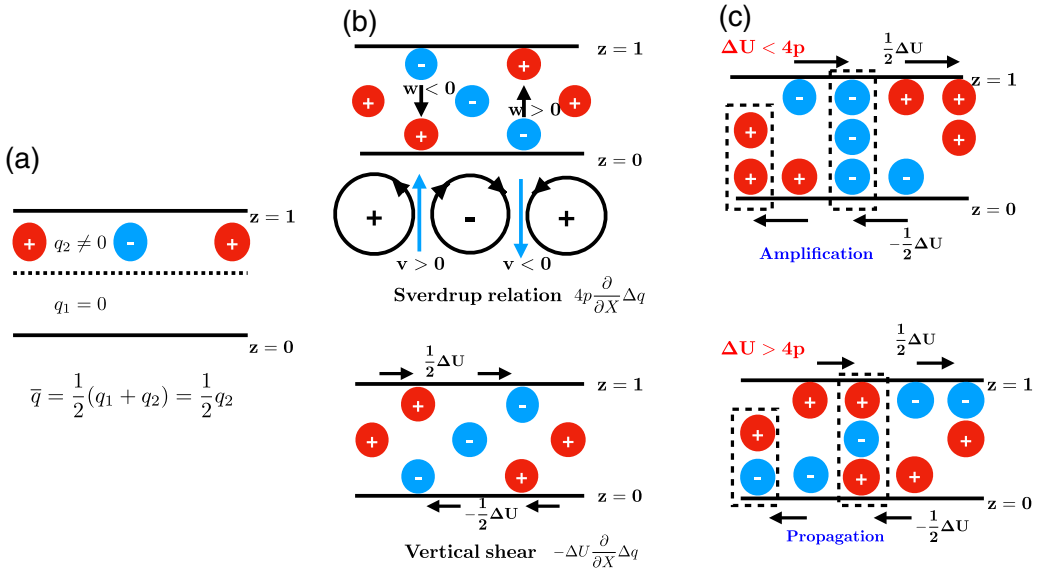


**FIGURE 4** A description of the instability generated by the combination of vertical shear and the Sverdrup relation in the planetary-scale atmosphere. Here, red (blue) circles represent positive (negative) $q$, which can be understood as the planetary-scale vorticity. Thus, a red (blue) circle describes cyclonic (anticyclonic) motion. (a) First, there exists an initial perturbation, $q_2 \neq 0$ and $q_1 = 0$. Hence, the barotropic mode $\frac{1}{2}(q_1 + q_2)$ has a nonzero value ($\frac{1}{2}q_2$). The barotropic mode can be interpreted as the $q$ at $z = \frac{1}{2}$. (b) Between the positive (negative) $\overline{q}$ and the negative (positive) $\overline{q}$, positive (negative) meridional velocity $v$ is induced. Due to the Sverdrup relation, the positive (negative) $v$ leads to a negative (positive) $w$ at $z = 1/2$. Considering that $\partial q/\partial\tau \propto -\partial w/\partial z$ and $w = 0$ at $z = 0, 1$, the negative (positive) $w$ at $z = 1/2$ induces negative (positive) $q_1$ and positive (negative) $q_2$. On the other hand, the effect of the vertical shear, which can be seen as the horizontal advection by $\frac{1}{2}\Delta U$ at the upper level ($z = 3/4$) and by $-\frac{1}{2}\Delta U$ at the lower level ($z = 1/4$), induces positive $q_1$ and negative $q_2$ at the same horizontal position with the negative $w$ from the Sverdrup relation. Thus the two processes, the Sverdrup relation and the vertical shear, are opposite each other. Here, the comparison between $\Delta U$ and $4p$ determines which process is more dominant. (c) When $\Delta U < 4p$ ($\Delta U > 4p$), the Sverdrup relation (the shear effect) is larger. With advection by the vertical shear, the perturbation field induced by the Sverdrup relation (the shear effect) amplifies exponentially (propagates as a wave) [Colour figure can be viewed at wileyonlinelibrary.com]

is positive (negative) between the positive (negative) $\overline{q}$ and negative (positive) $\overline{q}$. The Sverdrup relation at $z = 1/2$ is simplified as $-w/H = \beta_L v$, because $\partial w/\partial z = 0$ at $z = 1/2$. Thus, positive (negative) $v$ relates to negative (positive) $w$.

The negative $w$ at $z = 1/2$ implies $\partial w/\partial z > 0$ at $z = 3/4$ and $\partial w/\partial z < 0$ at $z = 1/4$, considering the two boundary conditions $w = 0$ at $z = 0, 1$. Because $\partial q/\partial \tau \propto -\partial w/\partial z$, the negative $w$ at $z = 1/2$ induces a baroclinic mode showing negative vorticity in the upper layer and positive in the lower layer. Similarly, the positive $w$ at $z = 1/2$ leads to a baroclinic mode that has positive vorticity in the upper layer and negative vorticity in the lower layer. On the other hand, there is another effect to induce baroclinic modes by the vertical shear of the mean wind. Here, the upper layer velocity is $\frac{1}{2}\Delta U$ and the lower layer one $-\frac{1}{2}\Delta U$. Following the baroclinic wind, the initial disturbance induces a baroclinic mode that is opposite to the one from the Sverdrup relation (Figure 4b). Now, we have to ask which process is larger, which determines the condition for instability. When $\Delta U < 4p$, the overall induced baroclinic mode is similar to the one from the Sverdrup relation. The induced baroclinic mode is again advected by the baroclinic wind, where positive (negative) anomalies are added to the existing positive (negative) ones. This describes the amplification of the initial barotropic disturbance. On the other hand, when $\Delta U > 4p$, positive (negative) anomalies move toward negative (positive) ones owing to the baroclinic wind and push them away, which generates wave propagation (Figure 4c).

### 5.2.2 | Activity of synoptic eddies

The diffusivity $K$ is introduced to parameterize the activity of synoptic eddies on the planetary scale. For growing waves ($\sigma_{1,2}$), the larger diffusivity induces wave propagation that differs from the mean wind ($\overline{U}$). In particular, when the memory is not too large ($r = 0.5$) and the diffusivity is large, the growing wave described by $\sigma_1$ becomes almost stationary or moves slowly westward. We can see that the activity of synoptic eddies is crucial to generate counter-propagating waves against the mean wind. Previous research (Colucci, 1985; Nakamura and Wallace, 1993; Nakamura *et al.*, 1997) suggests that the effect of synoptic-scale baroclinic eddies is crucial for the development of planetary-scale blocking patterns. Recent research describing atmospheric blocking as a traffic jam also emphasizes the role of cyclogenesis in increasing local wave activity in the large-scale atmosphere (Nakamura and Huang, 2018). The complex behavior of synoptic eddies is parameterized by the diffusivity $K$ and the memory time-scale $r$. A growing mode opposing the zonal mean wind is required to have large $K$, which is consistent with previous observations and numerical simulations emphasizing the role of synoptic eddies on the development of planetary-scale waves.

The influence of large $K$ also induces unstable eastward-propagating waves that are faster than the mean wind. Along with stationary unstable waves, there are travelling waves when a background field with an optimal wind shear is unstable. The existence of travelling planetary-scale waves during blocking has been suggested in several previous studies based on reanalysis data (Hansen and Chen, 1982; Lejenas and Doos, 1987; Lejenäs and Madden, 1992). The current research suggests an elegant way to explain the generation of planetary-scale waves propagating eastward with respect to the mean wind.

## 5.3 | Comparison with observations and numerical simulations

There are numerous articles suggesting that the origin of the low-frequency variability of the large-scale atmosphere is due to nonlinear interactions between planetary-scale waves and synoptic-scale ones (Gall *et al.*, 1979; MacVean, 1985; Robinson, 1991). The linearization of the primitive equations leads to the Laplace tidal equation, the main time-scale of which is half a day, determined by the Earth's rotation rate (Lindzen, 1967), which is not adequate to explain the major time-scales of planetary-scale waves. Gall *et al.* (1979) suggests that planetary-scale waves grow due to the interaction of synoptic-scale waves with the local mean flow instead of wave–wave interactions. Using a hemispheric spectral model with no external forcing, long wave growth and low-frequency variability is generated (MacVean, 1985; Robinson, 1991). Furthermore, a spectral energetic analysis of atmospheric blocking shows that the Atlantic block is caused by the nonlinear interaction of baroclinic cyclone-scale waves with ultralong waves (Hansen and Chen, 1982). Stationary and travelling planetary-scale waves are observed with larger magnitude during Northern Hemisphere blocking (Lejenas and Doos, 1987).

Our article includes the nonlinear contribution of synoptic-scale eddies through eddy-memory effects in the horizontal heat flux acting as a consequence of wave–mean flow interaction. The time accumulation of the baroclinicity in the delay integral makes it possible to generate propagating waves in the heat equation by transforming the parabolic structure to a hyperbolic one. The resulting wave equation contains planetary-scale waves propagating westward and eastward with respect to the mean westerly wind. With the increase of diffusivity $K$, the fastest growing mode could be almost stationary or move

westward slowly, which could block the mean wind eventually. At the same time, eastward-propagating waves can grow in time, possibly leading to planetary-scale wiggles.

## 5.4 | Weakening baroclinicity and atmospheric blocking

The most important factor of midlatitude weather is the meridional temperature gradient, because it controls the structure of midlatitude jets, including their speed and vertical shear. Thus, the way global warming changes midlatitude weather is strongly associated with the relationship between global warming and the meridional temperature gradient. Recent research argues that the increase of extreme weather is closely related to a decrease of the meridional temperature gradient, caused mainly by Arctic amplification under global warming (see Francis and Vavrus, 2012, which, in particular, focuses on levels below 500 mb). In contrast, the meridional temperature gradient in the upper atmosphere turns out to increase under global warming, which can be explained by upper tropospheric warming in tropical areas (Shaw *et al.*, 2016; Lee *et al.*, 2019). At the same time, it is hard to make a concrete conclusion on the impact of global warming in the midlatitudes, due to the nonstationarity of the climate system and the non-negligible magnitude of background noise (Barnes and Screen, 2015; Blackport and Screen, 2020). Based on a finite length of observation data, it might be hard to obtain a consensus conclusion of how global warming influences midlatitude jets without a solid dynamical theory (Wallace *et al.*, 2014).

The characteristics of synoptic eddies in the midlatitudes are summarized by poleward heat flux and momentum flux (Simmons and Hoskins, 1978). Interestingly, poleward heat flux generated by synoptic eddies is maximized at lower levels, but momentum flux at upper levels (Edmon *et al.*, 1980). Furthermore, the two turbulent fluxes are dynamically separated, thus their correlation is weak (Thompson and Woodworth, 2014). In the Southern Hemisphere, the SAM (Southern Annular Mode), which is strongly associated with upper-level momentum flux, and the BAM, related to poleward heat flux, show different variability (Thompson and Barnes, 2014). The planetary geostrophic equation in the current article focuses mainly on the role of the poleward heat flux induced by synoptic eddies as a thermal forcing, and hence the two-layer model describes fluid dynamics in lower levels. Here, it is reasonable to consider a weakening of the meridional temperature gradient near the surface where the poleward heat flux is maximized. The main question is how the lower-level weakening of meridional temperature gradient in the midlatitudes can influence synoptic eddies, planetary geostrophic motion, and their interactions.

However, the growth of planetary-scale waves cannot be explained by traditional baroclinic instability theory, which requires the meridional temperature gradients to be larger than a threshold. The observation that the intensification of a planetary-scale fluctuation is related to a decrease of the meridional temperature gradient is against our understanding of classical synoptic baroclinic instability. It suggests that a different mechanism is required to rationalize the recent increase of planetary-scale fluctuations causing extreme weather in the midlatitudes.

The instability found here in planetary-scale motions is a potential candidate to explain the observations. Planetary-scale instability needs the vertical shear of the mean wind to be no larger than a threshold. Without vertical shear, there is no instability, but a strong shear also prevents instability. An optimal shear exists for the growth of planetary-scale waves. According to our normal-mode analysis, the threshold is represented by the combination of the vertical static stability and the planetary $\beta$ effect. The threshold is proportional to $p = \frac{1}{8}\beta_L SH$, where larger $p$ provides a better condition for instability. The factor $(SH)$ is proportional to the vertical static stability. Recent research shows that global warming leads to an increase of bulk measures of dry static stability (Frierson, 2006), even though it varies regionally (Simmonds and Li, 2021). Therefore, under global warming, the meridional temperature gradient in high latitudes decreases and the dry static stability increases. The threshold $p$ increases and the baroclinicity $\Delta U$ decreases under global warming. Thus, global warming provides better conditions for planetary-scale instability to occur ($\Delta U < 4p$). However, global warming induces poleward shifts of tropospheric zonal jets (Lorenz and DeWeaver, 2007; Lu *et al.*, 2008), which contributes to a decrease of the $\beta$ effect in the center of jets.

The hypothesis that the decrease of the meridional temperature gradient $T_y$ leads to more frequent occurrence of atmospheric blocking was tested in an idealized GCM by Hassanzadeh *et al.* (2014). In particular, they focused on the relationship between reducing $T_y$ and the frequency of blocking. Despite the decrease of the zonal mean wind, the model results show a decline of atmospheric blocking occurrence. According to the dispersion relation (Equation 31), planetary-scale waves propagate westward with respect to the mean wind when

$$\frac{K}{r}(k^2 + l^2) > \frac{1}{4}r^2 + \frac{1}{16}b^2k^2.$$

Large $K$ implies that strong synoptic wave activity is required. The activity of synoptic waves in the midlatitudes

is strongly related to the traditional baroclinic instability, which requires strong baroclinicity measured by the meridional temperature gradient $T_y$. Barry *et al.* (2002) suggest a scaling of the poleward heat flux $\overline{v'T'}$ proportional to $T_y^{8/5}$, which implies that $K \propto T_y^{3/5}$ under our parameterization of the meridional heat flux. Thus, stationary or westward-propagating planetary-scale waves need a certain degree of meridional temperature gradient. Two opposing effects coexist. The unstable background for planetary-scale waves requires a lower meridional temperature gradient, which hinders provision of enough synoptic wave activity to the planetary-scale atmosphere. Therefore, the relative magnitude of both effects will determine whether Arctic amplification leads to more frequent occurrence of atmospheric blocking.

## 5.5 | Limitations

The normal-mode analysis based on the planetary-scale heat equation has its limitations. The memory kernel chosen in this research is a finite memory one, $\kappa(t-t') = \exp\left[-(t-t')/r\right]$. It is an approximation of the nonlinear interactions between synoptic waves and planetary-scale motions. The choice of the finite-time kernel was tested in numerical simulations of ocean eddies to explain the quasi-oscillatory behavior of the ocean mean field (Manucharyan *et al.*, 2017) and the large-scale atmospheric heat flux known as BAM can be explained by a stochastic oscillator derived by the finite eddy memory (Moon *et al.*, 2021). It is known that the midlatitude jet is self-maintained by eddy–mean interactions (Robinson, 2000; 2006). The generation of synoptic eddies is achieved by destabilizing the jets, but saturated eddies give their energy back to the jets to recover the original status of the jets. The eddy life cycle in the midlatitudes has a finite time-scale. Thus, the eddies inherited by the time evolution of jets should have a finite time-scale. However, the self-maintenance of the jets is based on a zonally averaged field. We apply the same kernel in every local area. The memory kernel is an approximation of the nonlinear behavior of synoptic eddies, which could vary, depending on the area and the temporal change of the mean state. We might need a more complicated integral kernel for a more detailed description of the nonlinear interactions between synoptic eddies and planetary-scale motions.

When the baroclinicity $\Delta U$ is smaller than $4p$, planetary-scale instability can induce the growth of waves. The growth rate increases with the zonal wavenumber $k$ (De Verdiere, 1986). There is no shortwave cutoff in terms of the growth rate, which might be unrealistic. Even though we can find the conditions for instability, we cannot identify the dominant spatial pattern emerging as a consequence of the instability. It is expected that a more complicated and realistic integral kernel could indicate more realistic growth rates and aid the identification of dominant spatial scales.

In this article, we provide conditions for planetary-scale instability under zonally symmetric conditions. In the Northern Hemisphere, the large-scale atmospheric dynamics is influenced by zonally asymmetric thermal and orographic forcing (Brayshaw *et al.*, 2011; Garfinkel *et al.*, 2020) and atmospheric blocking shows regional characteristics. Specific areas are preferred for the development of atmospheric blocking (Barriopedro *et al.*, 2006). Our model is not able to capture this dynamics, hence it is hard to apply the current theoretical results to situations in the Northern Hemisphere. We need to introduce local instability theory with zonally asymmetric thermal forcing to be closer to a realistic situation in the Northern Hemisphere (Pierrehumbert, 1984). Furthermore, atmospheric blocking and related phenomena contain various scales and their nonlinear interactions lead to coherent structures (Haines and Marshall, 1987). In particular, synoptic-scale waves can induce resonance (Petoukhov *et al.*, 2013) and evolve due to nonlinear dynamics (Luo *et al.*, 2019; Luo and Zhang, 2020). The current model does not contain all of these features. How planetary-scale backgrounds are associated with the nonlinear development of synoptic waves is a topic for future research.

We rely on the simplest treatment of the vertical structure of planetary-scale motions necessary for simple analytical expressions. In reality, the simple two-layer model is not enough to describe the vertical structure and movement of planetary-scale waves. According to Charney and Drazin (1990), only long waves generated in the lower troposphere can propagate into the stratosphere. The current research is not able to describe the vertical movement of planetary-scale waves. In the future, instead of layered models, a vertically continuous model should be considered to investigate the vertical propagation of planetary waves. Here, the planetary waves do not originate from a linear response to boundary thermal forcing. They are generated from nonlinear interactions between synoptic waves and planetary-scale motions. A continuous model in the vertical domain could provide insight into how the nonlinear activity of synoptic eddies can induce planetary-scale waves propagating towards the stratosphere (Scinocca and Haynes, 1998).

Finally, the current theoretical research would benefit from a determination of the eddy-memory scale $r$ and the turbulent diffusivity $K$ from observations or numerical simulations. The dynamic features of synoptic eddies are parameterized as two coefficients $r$ and $K$. Considering the

complicated and turbulent nature of synoptic eddies, $r$ and $K$ can depend on numerous factors. At the same time, the analysis is performed for specific values of $r$ and $K$. Further research should consider a parameter sweep along, with a nonlinear analysis of the reduced set of equations, and how to deduce $r$ and $K$ and trace the spatial and temporal variability of the two coefficients using observations and numerical simulations.

## 6 | CONCLUSION

Planetary-scale fluctuations in the large-scale atmosphere are quite crucial for many important phenomena, including atmospheric blocking and eastward-propagating planetary-scale waves. Previous research suggests that these phenomena are the result of interactions between synoptic and planetary-scale waves.

Here we consider a parameterization of the synoptic-scale heat flux through the planetary-scale baroclinicity based on the eddy-memory effect. Instead of an instantaneous relationship, the synoptic-scale poleward heat flux is assumed to be the result of past accumulations of the planetary-scale baroclinicity. The planetary-scale motions are approximated by a forced heat equation with classical dynamic balances, which means that there is only one time derivative in the governing equations. Thus, the linear dynamics cannot induce wave propagation. A perturbation is only advected by the mean velocity. The introduction of a finite-time kernel for the eddy-memory effect transforms the heat equation into a damped wave equation, which admits propagating waves.

The introduction of a vertical shear proportional to the meridional temperature gradient allows the interaction of vertical layers and then develops conditions for planetary-scale instability. In a two-layer model, the simplest representation of the sheared flow, the condition for instability is represented by a threshold of vertical shear, which is determined by the combination of the planetary beta effect and static stability. Interestingly, a smaller shear invokes two unstable waves, one of which is almost stationary and the other eastward-propagating. In particular, the growth of the stationary wave may be relevant to the onset of atmospheric blocking. Even in a highly simplified setting, several observations support this result. The current global warming, causing Arctic amplification and an increase in dry static stability, provides more preferable conditions for the instability, which is consistent with recent planetary-scale fluctuations causing extreme weather in many areas. However, we have to be cautious, as the overall planetary-wave changes due to climate change will be affected by other processes as well.

## ACKNOWLEDGEMENTS

W.M. acknowledges the support of Swedish Research Council Grant No. 638-2013-9243. G.E.M. acknowledges support from the United States Office of Naval Research award N00014-19-1-2421. H.D. acknowledges support by the Netherlands Earth System Science Centre (NESSC), financially supported by the Ministry of Education, Culture and Science (OCW), Grant No. 024.002.001.

## AUTHOR CONTRIBUTIONS

**Woosok Moon:** conceptualization; data curation; formal analysis; investigation; methodology; project administration; validation; visualization; writing – original draft; writing – review and editing. **Georgy E. Manucharyan: Henk A. Dijkstra:** conceptualization; investigation; methodology; project administration; validation; writing – review and editing.

## ORCID

*Woosok Moon* https://orcid.org/0000-0003-4025-8682

## REFERENCES

Barnes, E.A. and Screen, J.A. (2015) The impact of Arctic warming on the midlatitude jet-stream: can it? Has it? Will it? *Wiley Interdisciplinary Reviews: Climate Change*, 6(3), 277–286.

Barriopedro, D., Garcia-Herrera, R., Lupo, A.R. and Hernandez, E. (2006) A climatology of Northern Hemisphere blocking. *Journal of Climate*, 19(6), 1042–1063.

Barry, L., Craig, G.C. and Thuburn, J. (2002) Poleward heat transport by the atmospheric heat engine. *Nature*, 415(6873), 774–777.

Blackport, R. and Screen, J.A. (2020) Insignificant effect of Arctic amplification on the amplitude of midlatitude atmospheric waves. *Science Advances*, 6(8), eaay2880.

Brayshaw, D.J., Hoskins, B. and Blackburn, M. (2011) The basic ingredients of the North Atlantic storm track. Part 2: sea surface temperatures. *Journal of the Atmospheric Sciences*, 68(8), 1784–1805.

Charney, J.G. (1947) The dynamics of long waves in a baroclinic westerly current. *Journal of Meteorology*, 4(5), 136–162.

Charney, J.G. and Drazin, P.G. (1990). Propagation of planetary-scale disturbances from the lower into the upper atmosphere. In:, *The Atmosphere? A Challenge*, pp. 295–321: Boston, MA: Springer.

Cohen, S.J. (1990) Bringing the global warming issue closer to home: the challenge of regional impact studies. *Bulletin of the American Meteorological Society*, 71(4), 520–526.

Colucci, S.J. (1985) Explosive cyclogenesis and large-scale circulation changes: implications for atmospheric blocking. *Journal of Atmospheric Sciences*, 42(24), 2701–2717.

De Verdiere, A.C. (1986) On mean flow instabilities within the planetary geostrophic equations. *Journal of Physical Oceanography*, 16(11), 1981–1984.

Dolaptchiev, S.I. and Klein, R. (2009) Planetary geostrophic equations for the atmosphere with evolution of the barotropic flow. *Dynamics of Atmospheres and Oceans*, 46(1–4), 46–61.

Eady, E.T. (1949) Long waves and cyclone waves. *Tellus*, 1(3), 33–52.
Edmon, J.H.J., Hoskins, B.J. and McIntyre, M.E. (1980) Eliassen–Palm cross sections for the troposphere. *Journal of Atmospheric Sciences*, 37(12), 2600–2616.
Francis, J.A. and Vavrus, S.J. (2012) Evidence linking Arctic amplification to extreme weather in midlatitudes. *Geophysical Research Letters*, 39(6), L06801.
Francis, J.A. and Vavrus, S.J. (2015) Evidence for a wavier jet stream in response to rapid Arctic warming. *Environmental Research Letters*, 10(1), 014 005.
Frierson, D.M.W. (2006) Robust increases in midlatitude static stability in simulations of global warming. *Geophysical Research Letters*, 33(24), L24816.
Gall, R., Blakeslee, R. and Somerville, R.C.J. (1979) Cyclone-scale forcing of ultralong waves. *Journal of the Atmospheric Sciences*, 36(9), 1692–1698.
Garfinkel, C.I., White, I., Gerber, E.P., Jucker, M. and Erez, M. (2020) The building blockings of Northern Hemisphere wintertime stationary waves. *Journal of Climate*, 33(13), 5611–5633.
Ghil, M. and Mo, K. (1991a) Intraseasonal oscillations in the global atmosphere. Part I: northern hemisphere and tropics. *Journal of the Atmospheric Sciences*, 48(5), 752–779.
Ghil, M. and Mo, K. (1991b) Intraseasonal oscillations in the global atmosphere. Part II: southern hemisphere. *Journal of the Atmospheric Sciences*, 48(5), 780–790.
Haines, K. and Marshall, J. (1987) Eddy-forced coherent structures as a prototype of atmospheric blocking. *Quarterly Journal of the Royal Meteorological Society*, 113(476), 681–704.
Hansen, A.R. and Chen, T.C. (1982) A spectral energetics analysis of atmospheric blocking. *Monthly Weather Review*, 110(9), 1146–1165.
Hassanzadeh, P., Kuang, Z. and Farrell, B.F. (2014) Responses of midlatitude blocks and wave amplitude to changes in the meridional temperature gradient in an idealized dry GCM. *Geophysical Research Letters*, 41(14), 5223–5232.
Held, I.M. and Suarez, M.J. (1994) A proposal for the intercomparison of the dynamic cores of atmospheric general circulation models. *Bulletin of the American Meteorological Society*, 75(10), 1825–1830.
Hurrell, J.W., Kushnir, Y., Ottersen, G. and Visbeck, M. (2003) An overview of the North Atlantic oscillation. *Geophysical Monograph–American Geophysical Union*, 134, 1–36.
Jüling, A., Dijkstra, H.A., Hogg, A.M. and Moon, W. (2020) Multidecadal variability in the climate system: phenomena and mechanisms. *The European Physical Journal Plus*, 135(6), 1–22.
Lee, S.H., Williams, P.D. and Frame, T.H. (2019) Increased shear in the North Atlantic upper-level jet stream over the past four decades. *Nature*, 572(7771), 639–642.
Lejenas, H. and Doos, R. (1987) The behaviour of the stationary and travelling planetary-scale waves during blocking–a northern hemisphere data study. *Journal of the Meteorological Society of Japan. Series II*, 65(5), 709–725.
Lejenäs, H. and Madden, R.A. (1992) Traveling planetary-scale waves and blocking. *Monthly Weather Review*, 120(12), 2821–2830.
Lindzen, R.S. (1967) Thermally driven diurnal tide in the atmosphere. *Quarterly Journal of the Royal Meteorological Society*, 93(395), 18–42.
Lorenz, D.J. and DeWeaver, E.T. (2007) Tropopause height and zonal wind response to global warming in the IPCC scenario integrations. *Journal of Geophysical Research: Atmospheres*, 112(D10), 3470–3484.
Lu, J., Chen, G. and Frierson, D.M. (2008) Response of the zonal mean atmospheric circulation to El Niño versus global warming. *Journal of Climate*, 21(22), 5835–5851.
Luo, D., Zhang, W., Zhong, L. and Dai, A. (2019) A nonlinear theory of atmospheric blocking: a potential vorticity gradient view. *Journal of the Atmospheric Sciences*, 76(8), 2399–2427.
Luo, D. and Zhang, W. (2020) A nonlinear multiscale theory of atmospheric blocking: eastward and upward propagation and energy dispersion of tropospheric blocking wave packets. *Journal of the Atmospheric Sciences*, 77(12), 4025–4049.
MacVean, M.K. (1985) Long-wave growth by baroclinic processes. *Journal of the Atmospheric Sciences*, 42(11), 1089–1101.
Manabe, S. and Strickler, R.F. (1964) Thermal equilibrium of the atmosphere with a convective adjustment. *Journal of Atmospheric Sciences*, 21(4), 361–385.
Manucharyan, G.E., Thompson, A.F. and Spall, M.A. (2017) Eddy memory mode of multidecadal variability in residual-mean ocean circulations with application to the Beaufort gyre. *Journal of Physical Oceanography*, 47(4), 855–866.
Moon, W. and Cho, J. (2020) A balanced state consistent with planetary-scale motion for quasigeostrophic dynamics. *Tellus A: Dynamic Meteorology and Oceanography*, 72(1), 1–12.
Moon, W., Manucharyan, G.E. and Dijkstra, H.A. (2021) Eddy memory as a cause of intra-seasonal variability of the southern hemisphere baroclinic annular mode. *Quarterly Journal of the Royal Meteorological Society*, 147, 2395–2408.
Nakamura, N. and Huang, C.S. (2018) Atmospheric blocking as a traffic jam in the jet stream. *Science*, 361(6397), 42–47.
Nakamura, H., Nakamura, M. and Anderson, J.L. (1997) The role of high- and low-frequency dynamics in blocking formation. *Monthly Weather Review*, 125(9), 2074–2093.
Nakamura, H. and Wallace, J.M. (1993) Synoptic behavior of baroclinic eddies during the blocking onset. *Monthly Weather Review*, 121(7), 1892–1903.
Pedlosky, J. (2013) *Geophysical Fluid Dynamics*. New York, NY: Springer Science & Business Media.
Petoukhov, V., Rahmstorf, S., Petri, S. and Schellnhuber, H.J. (2013) Quasiresonant amplification of planetary waves and recent northern hemisphere weather extremes. *Proceedings of the National Academy of Sciences*, 110(14), 5336–5341.
Phillips, N.A. (1951) A simple three-dimensional model for the study of large-scale extratropical flow patterns. *Journal of Meteorology*, 8(6), 381–394.
Phillips, N.A. (1954) Energy transformations and meridional circulations associated with simple baroclinic waves in a two-level, quasigeostrophic model. *Tellus*, 6(3), 274–286.
Phillips, N.A. (1963) Geostrophic motion. *Reviews of Geophysics*, 1(2), 123–176.
Pierrehumbert, R.T. (1984) Local and global baroclinic instability of zonally varying flow. *Journal of the Atmospheric Sciences*, 41(14), 2141–2162.
Pierrehumbert, R.T. and Swanson, K.L. (1995) Baroclinic instability. *Annual Review of Fluid Mechanics*, 27(1), 419–467.
Pithan, F. and Mauritsen, T. (2014) Arctic amplification dominated by temperature feedbacks in contemporary climate models. *Nature Geoscience*, 7(3), 181–184.

Robinson, W.A. (1991) The dynamics of low-frequency variability in a simple model of the global atmosphere. *Journal of the Atmospheric Sciences*, 48(3), 429–441.

Robinson, W.A. (2000) A baroclinic mechanism for the eddy feedback on the zonal index. *Journal of the Atmospheric Sciences*, 57(3), 415–422.

Robinson, W.A. (2006) On the self-maintenance of midlatitude jets. *Journal of the Atmospheric Sciences*, 63(8), 2109–2122.

Screen, J.A. and Simmonds, I. (2014) Amplified midlatitude planetary waves favour particular regional weather extremes. *Nature Climate Change*, 4(8), 704–709.

Serreze, M.C., Barrett, A.P., Stroeve, J.C., Kindig, D.N. and Holland, M.M. (2009) The emergence of surface-based Arctic amplification. *The Cryosphere*, 3(1), 11.

Simmonds, I. and Li, M. (2021) Trends and variability in polar sea ice, global atmospheric circulations, and baroclinicity. *Annals of the New York Academy of Sciences*, 1504(1), 167–186.

Simmons, A.J. and Hoskins, B.J. (1978) The life cycles of some nonlinear baroclinic waves. *Journal of Atmospheric Sciences*, 35(3), 414–432.

Shaw, T.A., Baldwin, M., Barnes, E.A., Caballero, R., Garfinkel, C.I., Hwang, Y.T., Li, C., O'Gorman PA, Riviere G, Simpson IR and Voigt A. (2016) Storm track processes and the opposing influences of climate change. *Nature Geoscience*, 9(9), 656–664.

Scinocca, J.F. and Haynes, P.H. (1998) Dynamical forcing of stratospheric planetary waves by tropospheric baroclinic eddies. *Journal of the Atmospheric Sciences*, 55(14), 2361–2392.

Thompson, D.W. and Barnes, E.A. (2014) Periodic variability in the large-scale southern hemisphere atmospheric circulation. *Science*, 343(6171), 641–645.

Thompson, D.W. and Woodworth, J.D. (2014) Barotropic and baroclinic annular variability in the Southern Hemisphere. *Journal of the Atmospheric Sciences*, 71(4), 1480–1493.

Thompson, D.W. and Wallace, J.M. (1998) The Arctic Oscillation signature in the wintertime geopotential height and temperature fields. *Geophysical Research Letters*, 25(9), 1297–1300.

Wallace, J.M., Held, I.M., Thompson, D.W.J., Trenberth, K.E. and Walsh, J.E. (2014) Global warming and winter weather. *Science*, 343(6172), 729–730.

Woollings, T., Hannachi, A. and Hoskins, B. (2010) Variability of the North Atlantic eddy-driven jet stream. *Quarterly Journal of the Royal Meteorological Society*, 136(649), 856–868.

**How to cite this article:** Moon, W., Manucharyan, G.E. & Dijkstra, H.A. (2022) Baroclinic instability and large-scale wave propagation in a planetary-scale atmosphere. *Quarterly Journal of the Royal Meteorological Society*, 148(743), 809–825. Available from: https://doi.org/10.1002/qj.4232